Research Article Vol. 4, No. 1 / January 2017 / Optica 64

Polarization time of unpolarized light

Andriy Shevchenko,[1] Matthieu Roussey,[2] Ari T. Friberg,[2] and Tero Setälä[2,*]

[1]Department of Applied Physics, Aalto University, P.O. Box 13500, FI-00076 Aalto, Finland
[2]Institute of Photonics, University of Eastern Finland, P.O. Box 111, FI-80101 Joensuu, Finland
*Corresponding author: tero.setala@uef.fi

Received 14 July 2016; revised 21 November 2016; accepted 28 November 2016 (Doc. ID 270533); published 6 January 2017

Light produced by most natural and artificial sources is unpolarized or partially polarized. At any instant of time, however, such random light can be regarded as fully polarized, but the polarization state may vary drastically within short time intervals. This rate of change is another attribute that separates one unpolarized beam from another. Here, we study such polarization dynamics and, for the first time to our knowledge, measure the characteristic time, called the polarization time, in which the instantaneous polarization state stays essentially unaltered. The technique employs a polarization-sensitive Michelson interferometer and two-photon absorption detection valid for electromagnetic light, yielding superior femtosecond time resolution. We analyze two unpolarized light sources: amplified spontaneous emission from a fiber amplifier and a dual-wavelength laser source. The characterization of polarization dynamics can have significant applications in optical sensing, polarimetry, telecommunication, and astronomy, as well as in quantum and atom optics.

OCIS codes: (030.1640) Coherence; (260.5430) Polarization; (260.3160) Interference; (190.4180) Multiphoton processes.

https://doi.org/10.1364/OPTICA.4.000064

1. INTRODUCTION

Light fields may differ in their spectrum, intensity, and polarization, as well as in spatial, temporal, and spectral coherence properties. In addition, not all unpolarized light beams are equal. For example, the unpolarized state may be irreversible, as with thermal light, or full polarization may be recovered without absorption [1]. Artificial beams often exhibit reversible unpolarized states [2]. Yet, a practically unexplored feature that can distinguish two random light beams is their polarization dynamics, i.e., the temporal evolution of the instantaneous polarization state. For monochromatic light, the polarization ellipse and the associated polarization state are fixed at all times and no polarization dynamics occur. The same is true for random but fully polarized beams, whose intensity, however, may fluctuate. On the other hand, for most natural and many artificial light sources, which are partially polarized, the polarization ellipse varies randomly both in shape and orientation on a femtosecond scale. Two partially polarized beams, for example, may share identical degrees and average states of polarization, but the characteristic speeds at which the instantaneous polarization states change in time can be entirely different. The typical ultrafast polarization variations are impossible to observe directly even with the fastest existing photodetectors, as their response times are too long, on the order of 10 ps. This issue, along with the fact that a general theory of polarization dynamics in random light was introduced only very recently [3–5], has hampered the research progress and applications connected to this topic.

The time interval over which the instantaneous polarization state of fluctuating light does not change significantly is referred to as the polarization time [3–5] [see Fig. 1(a)]. Geometrically, it can be visualized as a period of time in which the instantaneous polarization state on the Poincaré sphere does not move far from its original position [3]. Mathematically, it can be quantified with polarization correlation functions involving intensity correlations of various polarization components [3–5]. Conceptually, the polarization time resembles the classical notion of coherence time but quantitatively differs substantially from it. For example, fully polarized light has an infinite polarization time, but the coherence time can be almost anything. The polarization time is a new quantity specifying the rate of the polarization-state fluctuations, and it can provide useful information on natural light sources and propagation media. Polarization dynamics may benefit research dealing with polarization fluctuations, e.g., polarization-mode dispersion in optical fibers [6], particle shape determination [7], polarimetric radar imaging [8], supercontinuum light [9], polarization beating for higher-order harmonic generation [10], vertical-cavity surface-emitting lasers [11], polarization chaos in laser diodes [12], and optical telecommunication [13], as well as polarimetry of stellar sources and thermal background radiation from the Big Bang [14–16]. Mapping the time-averaged polarization state of cosmic microwave background radiation has already provided us with new, groundbreaking information on the early universe, and the possibility of measuring dynamical characteristics of the polarization state of this radiation can open one more channel of information for further cosmological investigations. Further, the quantum-mechanical selection rules governing atomic and molecular transitions depend essentially on the polarization state of light [17,18], while the fluctuations in

fluorescence emission of single emitters yield information on their nanoscopic environment [19]. The polarization time can also be used to characterize pulsed beams, such as Poincaré beams, in which the polarization can go through all possible states within each pulse [20], and beams created by cascade emission of pairs of orthogonally polarized photons by quantum dots [21].

Here, we present the first measurement, to our knowledge, of the polarization time by analyzing two unpolarized, continuous-wave light beams: amplified spontaneous emission (ASE) from an Er-doped fiber amplifier, and the superposition of two independent, orthogonally polarized, equal-intensity narrowband laser beams. The technique is based on using two-photon absorption [22,23] in a GaAs photomultiplier tube [24,25] and a polarization-sensitive Michelson interferometer, which together provide the required femtosecond-scale time resolution. The method is valid effectively for any random or deterministic behavior of instantaneous polarization. A similar technique has recently been employed to measure the coherence time of random electromagnetic beams [26], and before that, its scalar analogue was applied to show photon bunching in thermal light [27], extra bunching in twin beams [28], and pulse compression by two-photon gain [29]. We note that the scalar approach is not adequate in the electromagnetic context, since the polarization dynamics give an essential contribution to the two-photon absorption signal [26]. In our approach, the polarization time is found by measuring the intensity auto- and cross-correlation functions of various polarization components of light with the help of two-photon absorption. Whereas these functions can be obtained also by other photodetection methods, e.g., based on second-harmonic generation [30,31], we consider our technique as flexible and readily adaptable to other spectral ranges and polarization time scales.

2. POLARIZATION DYNAMICS

At sufficiently short time intervals (of at least a few cycles), all random or deterministic light is fully polarized with a specific polarization state. For beam fields, this state can be characterized by the normalized instantaneous Poincaré vector [32] $\mathbf{s}(t) = [s_1(t), s_2(t), s_3(t)]$, where $s_i(t) = S_i(t)/S_0(t)$, with $i \in (1, 2, 3)$, are the time-dependent polarization-state Stokes parameters divided by the intensity. The quantities are given as

$$S_0(t) = I_x(t) + I_y(t), \tag{1}$$

$$S_1(t) = I_x(t) - I_y(t), \tag{2}$$

$$S_2(t) = I_{+45}(t) - I_{-45}(t), \tag{3}$$

$$S_3(t) = I_{\mathrm{RCP}}(t) - I_{\mathrm{LCP}}(t), \tag{4}$$

where $I_x(t)$ and $I_y(t)$ are the instantaneous intensities of the x- and y-polarized field components, $I_{+45}(t)$ and $I_{-45}(t)$ are the analogous quantities of the components polarized at an angle of $+45°$ and $-45°$, respectively, with respect to the x axis, while $I_{\mathrm{RCP}}(t)$ and $I_{\mathrm{LCP}}(t)$ represent the instantaneous intensities of the right-hand and left-hand circularly polarized fields. As depicted in Fig. 1(b), the vector $\mathbf{s}(t)$ specifies a point on the Poincaré sphere of unit radius. The evolution of the instantaneous polarization state over a time interval τ can be treated by considering the variation of $\mathbf{s}(t)$ to $\mathbf{s}(t+\tau)$. For a fully polarized beam of light

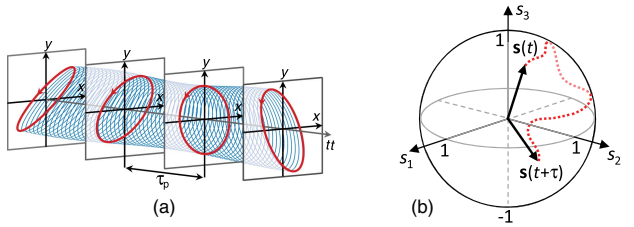

Fig. 1. Illustration of polarization dynamics. (a) The instantaneous polarization state represented by the red ellipses does not, on average, significantly change within the polarization time τ_p. (b) The instantaneous Poincaré vectors $\mathbf{s}(t)$ and $\mathbf{s}(t+\tau)$ determine how much the instantaneous polarization state changes on the Poincaré sphere within τ.

$\mathbf{s}(t)$ is fixed, while for an unpolarized beam, its time average, denoted by the brackets, vanishes, i.e., $\langle \mathbf{s}(t) \rangle = 0$.

How far, on average, the polarization state within τ moves on the Poincaré sphere may be quantified by the (polarization) correlation function [3]

$$\gamma_{\mathrm{P}}(\tau) = \frac{\langle [\mathbf{s}(t) \cdot \mathbf{s}(t+\tau)] S_0(t) S_0(t+\tau) \rangle}{\langle S_0(t) S_0(t+\tau) \rangle}. \tag{5}$$

The scalar product $\mathbf{s}(t) \cdot \mathbf{s}(t+\tau)$ varies from -1 to 1, corresponding to orthogonal and the same polarization states at times t and $t+\tau$. Thus, the higher its value is, the closer the polarization states are on the Poincaré sphere. In Eq. (5), the polarization states at t and $t+\tau$ are weighted by the associated intensities emphasizing the instants of time with high intensity and therefore of physical significance. The denominator of Eq. (5) serves to normalize the correlation function so that $\gamma_{\mathrm{P}}(0) = 1$ and $-1 \le \gamma_{\mathrm{P}}(\tau) \le 1$. We define the polarization time, τ_{p}, as a characteristic time interval over which the instantaneous polarization state remains, on average, essentially unaltered, i.e., $\gamma_{\mathrm{P}}(\tau)$ drops from $\gamma_{\mathrm{P}}(0)$ to $\gamma_{\mathrm{P}}(\tau_{\mathrm{p}}) = 0.5\gamma_{\mathrm{P}}(0)$, for instance. In Ref. [4], a quantity describing the redistribution rate of light energy between two orthogonal polarization states within τ was introduced. That function is monotonically related to the one in Eq. (5), and hence, the polarization time also represents a time period during which a significant amount of energy of a certain instantaneous polarization state transfers to the state orthogonal to it.

Rewriting the numerator in Eq. (5) leads to

$$\gamma_{\mathrm{P}}(\tau) = \frac{\sum_{n=1}^{3} \langle S_n(t) S_n(t+\tau) \rangle}{\langle S_0(t) S_0(t+\tau) \rangle}, \tag{6}$$

where the correlation functions of the Stokes parameters can be expressed as

$$\langle S_0(t) S_0(t+\tau) \rangle = C_{x,x}(\tau) + C_{x,y}(\tau) + C_{y,x}(\tau) + C_{y,y}(\tau), \tag{7}$$

$$\langle S_1(t) S_1(t+\tau) \rangle = C_{x,x}(\tau) - C_{x,y}(\tau) - C_{y,x}(\tau) + C_{y,y}(\tau), \tag{8}$$

$$\langle S_2(t) S_2(t+\tau) \rangle = C_{+45,+45}(\tau) - C_{+45,-45}(\tau) - C_{-45,+45}(\tau) + C_{-45,-45}(\tau), \tag{9}$$

$$\langle S_3(t) S_3(t+\tau) \rangle = C_{\mathrm{RCP,RCP}}(\tau) - C_{\mathrm{RCP,LCP}}(\tau) - C_{\mathrm{LCP,RCP}}(\tau) + C_{\mathrm{LCP,LCP}}(\tau). \tag{10}$$

Above, $C_{i,j}(\tau) = \langle I_i(t) I_j(t+\tau) \rangle$, with $(i, j) = (x, y, +45, -45, \text{RCP}, \text{LCP})$, is the intensity correlation function related to the polarization states indicated by the subscripts i and j. Thus, measuring all intensity correlation functions allows us to find $\gamma_P(\tau)$ and the associated polarization time τ_p. Note that the polarization correlation function in Eq. (6) is general, independent of the statistics of the light fluctuations, and it can also be used to treat deterministically changing polarization. In addition, the method works for both stationary and nonstationary beams, although it does not provide information on the type of instantaneous polarization states.

3. MEASUREMENT TECHNIQUE

The electromagnetic detection that we use necessitates polarization-selective optical elements, quarter-wave plates and polarizers, in the arms of the interferometer [see Fig. 2(a)]. With these elements, we can select any polarization component of interest from the incident beam. Our experimental setup is as follows. Light that we analyze is coupled into a single-mode optical fiber (OF) and delivered to the interferometer, where it is collimated with a lens [L1 in Fig. 2(a)] to form a beam. The collimated beam is split into two beams with a polarization-insensitive beam splitter (BS). Each of these beams, when propagating in the interferometer arm toward the mirror (M), passes first a quarter-wave plate (WP) and then a linear polarizer (P). If, for example, the fast axis of the wave plate and the transmission axis of the polarizer are aligned parallel to each other, the selected polarization is linear along the polarizer's transmission axis. If the wave plate is rotated with respect to the polarizer by an angle of 45° in the clockwise direction, the selected component is right-hand circularly polarized. After reflection from the mirrors, the beams again pass the polarizers and the wave plates and are combined by the beam splitter into a single beam. This beam is focused with another lens (L2) onto a GaAs photomultiplier tube (PT). The diameter of the light spot on the photodetector's surface is about 5 μm. The quadratic dependence of the photocurrent on the optical power P of unpolarized light at the interferometer input was obtained for $P < 2$ mW, indicating that the photomultiplier tube operates in the two-photon absorption regime. In the experiments, we used powers on the order of 0.1 mW. One of the mirrors M is connected to a piezoelectric transducer to allow gradual change of the length of one arm. The transducer operates with a step of 100 nm and has a scanning range of 2.7 cm. The length difference Δl of the arms determines the time difference $\tau = 2\Delta l/c$ appearing in Eq. (6).

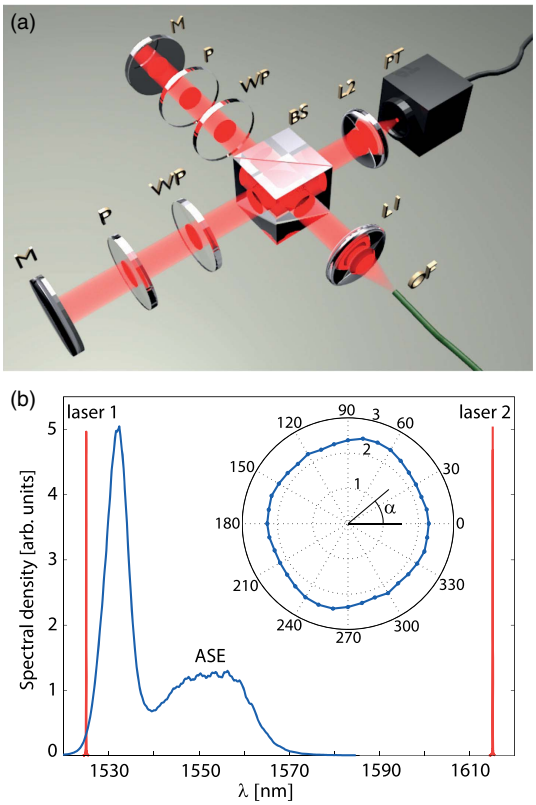

Fig. 2. Polarization-sensitive Michelson interferometer and the source spectra. (a) Experimental setup: OF, optical fiber; L1 and L2, lenses; BS, beam splitter; WP, quarter-wave plate; P, polarizer; M, mirror; and PT, photomultiplier tube. One of the mirrors is translated with a piezoelectric transducer to alter τ. (b) Measured spectra of the optical beams from the ASE of an Er-doped fiber amplifier (blue line) and two independent lasers (red line). The polar plot in the inset illustrates the dependence of the two-photon absorption signal on the orientation angle α of the linear polarization of incident light derived from the ASE.

The time resolution of this technique is determined by the energy gap E_g between the valence and the conduction band of the semiconductor and is equal to the lifetime $\hbar/E_g$ ($\hbar$ is the reduced Planck constant) of the virtual state via which the photon pairs are absorbed. For a photodetector used in our work (Hamamatsu H7421-50), the bandgap corresponds to the wavelength of $\lambda_g = 900$ nm. Thus, the wavelength range of the two-photon absorption regime is $900 < \lambda < 1800$ nm, and the temporal resolution is given by $\tau_r = \lambda_g/(2\pi c) < 1$ fs (c is the speed of light in a vacuum). The analysis of the two-photon absorption signal is shown in Appendix A.

4. EXPERIMENTAL RESULTS

Our aim is to measure the new characteristic quantity of light fields, the polarization time, for two unpolarized sources. The first source is unpolarized ASE of an Er-doped fiber amplifier. The field fluctuations of this source obey Gaussian statistics. The second source combines two independent, linearly polarized, single-mode lasers. The laser wavelengths are $\lambda_1 = 1525$ nm and $\lambda_2 = 1615$ nm, and the bandwidth of each of them is on the order of 100 MHz. The laser beams, aligned to have orthogonal polarizations, are combined into a single beam using a polarizing beam splitter. Since the lasers are independent, the resulting beam is unpolarized if the laser powers are equal. This source, being composed of two quasi-monochromatic beams, does not obey Gaussian statistics. Instead, it exhibits polarization beating, with the instantaneous polarization state periodically varying in time. The spectra of the two sources are shown in Fig. 2(b).

Setting the power of the ASE source well below 2 mW, we have measured the sensitivity of the two-photon absorption signal to the polarization of the incident light. The ASE beam was let through a polarizer and a half-wave plate and focused onto the photomultiplier. By rotating the plate, we changed the angle of the linear polarization, α, at the detector from 0° to 360° with 10° intervals. The result of these measurements is shown in the inset of Fig. 2(b) as a polar plot. The signal is seen to be nearly constant, with only a slight elevation at around $\alpha = 70°$. For our

measurements, however, this elevation is insignificant, and the detector response is considered as isotropic.

A. ASE Source

For the ASE source, the two-photon absorption signal was measured for a range of $\tau \in [-1130\ \text{fs}, 1130\ \text{fs}]$. Figure 3(a) shows the signal profiles obtained when the polarizers are aligned to transmit the (horizontal) x-polarized components in both arms (blue XX curve), the (vertical) y-components in both arms (red YY curve), and the x-component in one arm and y-component in the other arm (black XY curve). The red and blue curves oscillate rapidly, as illustrated also in the inset, where the curves are shown for a shorter τ interval. This oscillation corresponds to the last two terms in Eq. (A1). The signals show a major amplitude peak at $\tau = 0$ (the arms are of equal length) and two secondary peaks at $\tau = \pm 310$ fs. The secondary peaks are explained by the presence of two maxima in the ASE spectrum [see Fig. 2(b)]. Indeed, the spectral maxima are separated by about 25 nm, which causes temporal beating of the signal with a period of about 320 fs. The XX and YY curves nearly coincide, as the ASE light is unpolarized. The black XY curve does not oscillate, since the x-polarized and y-polarized field components arriving from the interferometer's arms to the detector do not correlate. Removing the fast oscillations from the curves with a Fourier-transform-based low-pass filtering [26], we obtain the signals $S_{ij}(\tau)$ of Eq. (A2). Together with the measured values of S_{1i} and S_{2i}, they result in the intensity correlation functions $C_{x,x}$, $C_{y,y}$, and $C_{x,y}$, shown in Fig. 3(b) with the blue XX, red YY, and black XY curves, respectively. The blue and red curves are peaked at $\tau = 0$, and the black curve is flat, as expected.

Selecting the right-hand and left-hand circular polarizations in the arms and repeating the measurements, we obtain the curves shown in Fig. 3(c). The overlap of the blue RR curve (right-hand polarization in both arms) with the red LL curve (left-hand polarizations in the arms) is remarkable, and the black RL curve (opposite circular polarizations in the arms) is flat. The corresponding intensity correlation functions found by Fourier-transform filtering the oscillating curves and applying Eq. (A.2) are shown in Fig. 3(d). They are similar to the curves in Fig. 3(b), as they should if the ASE light indeed is unpolarized. To obtain the complete set of the intensity correlation functions appearing in Eqs. (7–10), we also measured the functions $C_{+45,+45}$, $C_{-45,-45}$, and $C_{+45,-45}$. The resulting signal curves are shown in Fig. 3(e) and the corresponding intensity correlation functions in Fig. 3(f).

In the next step, the intensity correlation functions are inserted into Eqs. (7–10) to obtain the autocorrelation functions of the Stokes parameters. These functions also contain the intensity correlation functions $C_{y,x}(\tau)$, $C_{-45,+45}(\tau)$, and $C_{\text{LCP,RCP}}(\tau)$, which we did not measure. Instead, τ was scanned in each measurement from negative to positive values symmetrically around $\tau = 0$. Hence, in Eqs. (7–10), we replace each missing $C_{i,j}(\tau)$ with $C_{j,i}(-\tau)$. The resulting autocorrelation functions of the Stokes parameters are presented in Fig. 4(a).

Finally, we substitute the autocorrelation functions of the Stokes parameters into Eq. (6) and find the polarization correlation function $\gamma_P(\tau)$. This function is shown in Fig. 4(b). Its peak value at $\tau = 0$ differs slightly from the theoretically expected value of 1 due to imperfect alignment and the focusing of the polarized beams coming from the interferometer's arms onto the detector. The function $\gamma_P(\tau)$ is observed to decrease from $\gamma_P(0)$ to $\gamma_P(0)/2$ approximately in 115 fs. This time can be considered as the polarization time for the ASE source. Hence, on average, the unpolarized ASE light can be viewed effectively as polarized within a time interval of about 100-fs duration. Also, it can be regarded as polarized within any distance $l_p = \tau_p c = 35\ \mu\text{m}$ along the field propagation direction. The polarization time for this

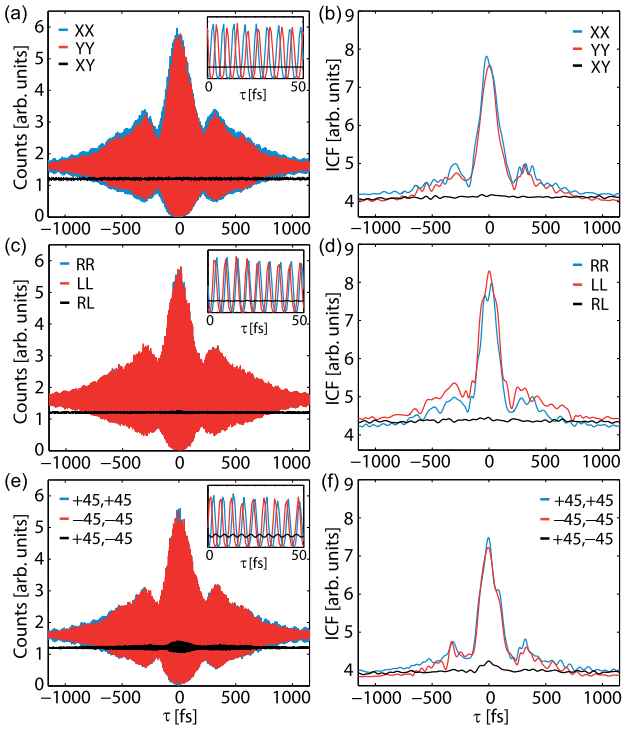

Fig. 3. Two-photon absorption counts (left) and the related intensity correlation functions (ICFs) (right) measured for ASE light. Curves in (a) and (b) were measured by selecting x-polarized fields in both arms of the interferometer (blue XX curves), y-polarized fields in both arms (red YY curves), and x- and y-polarized fields in different arms (black XY curve). The curves in (c) and (d) were measured by selecting right-hand circular polarizations in both arms (blue RR curves), left-hand circular polarizations in both arms (red LL curves), and right-hand and left-hand circular polarizations in different arms (black RL curves). In (e) and (f), the selected components are linearly polarized at an angle of +45° in both arms (blue +45, +45 curves), −45° in both arms (red −45, −45 curves), and +45° in one arm and −45° in the other arm, respectively (black +45, −45 curves). The insets in (a), (c), and (e) illustrate the oscillation of the measured signals at $\tau \in [0, 50\ \text{fs}]$.

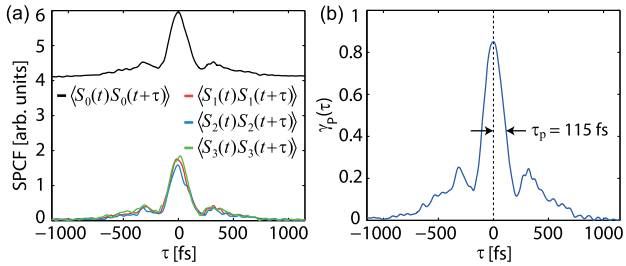

Fig. 4. Polarization dynamics of ASE light. (a) Autocorrelation functions of the Stokes parameters (SPCFs) and (b) the polarization correlation function $\gamma_P(\tau)$. The illustrated polarization time τ_p is determined from $\gamma_P(\tau_p) = \gamma_P(0)/2$.

unpolarized light source is seen to be on the order of the coherence time that can be measured for any of the polarization components of the field [26].

B. Laser Source

For the second light source, composed of two narrowband laser beams, we made the same measurements as for the ASE and obtained the signals shown in Figs. 5(a), 5(c), and 5(e). Each of the selected polarization components contains contributions from both lasers. Hence, each measured curve exhibits periodic amplitude modulation due to the wave-beating phenomenon. The observed modulation period, of about 90 fs, is indeed equal to the beating period $T = \lambda_2\lambda_1/(\lambda_2 - \lambda_1)c$. If we continued scanning the mirror so that τ would approach the coherence time of the lasers (~10 ns), the oscillation amplitudes would decrease. However, since 10 ns is five orders of magnitude longer than the measurement interval in Fig. 5, the oscillation amplitude in the measured three beating periods of each curve is the same. It can be seen that the signals obtained for identical polarizations in the arms, such as the XX and YY curves, have maximum amplitudes at $\tau = 0$, because the beating intensities from the interferometer arms come to the detector in phase. The black curves obtained for orthogonal polarizations in the arms also exhibit beating, but at $\tau = 0$ the signal is at minimum, since the intensity maxima arrive at the detector from the arms alternately. The fast oscillation observed in each black curve is explained by a coupling between the orthogonally polarized waves in the GaAs crystal. Since the crystal is optically anisotropic, the wave coming from one arm of the interferometer, $\mathbf{E}_i(t)$, acquires an orthogonal polarization component upon its interaction with the crystal, and this component interferes with the wave $\mathbf{E}_j(t+\tau)$ arriving from the other arm. As long as each arm contains both wavelength components, the waves $\mathbf{E}_i(t)$ and $\mathbf{E}_j(t+\tau)$ attain maximum correlation at $\tau = \pm T/2$. The contribution of this cross interference to two-photon absorption is proportional to $I_i(t)E_i(t)E_j^*(t+\tau)$ (see, e.g., Eqs. (19) and (20) in Ref. [33]). This contribution, however, is eliminated, together with the associated high-frequency oscillation by the Fourier-transform filtering applied in the next step. The fact that the red curve nearly coincides with the blue curve in each of three Figs. 5(a), 5(c), and 5(e) confirms that the analyzed two-laser beam is unpolarized.

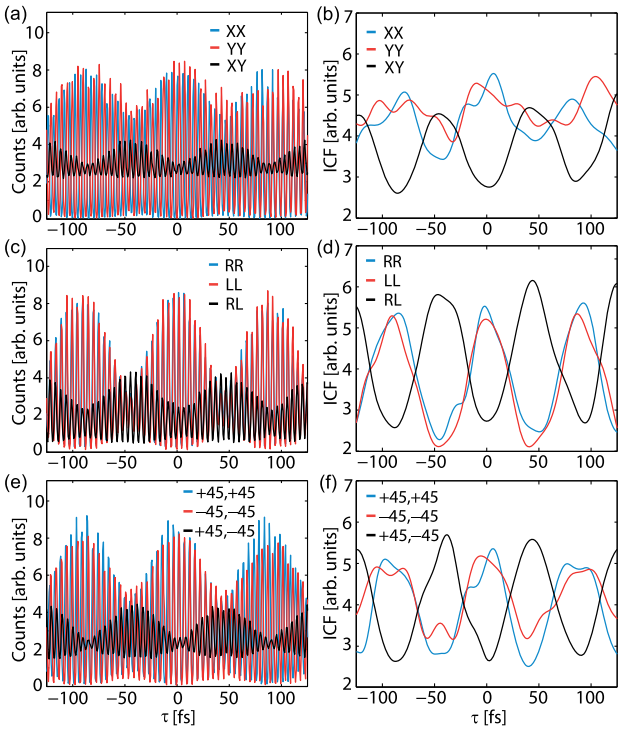

Fig. 5. Two-photon absorption counts (left) and the corresponding ICFs (right) measured for a two-laser beam. Curves in (a) and (b) were measured by selecting x-polarized fields in both arms of the interferometer (blue XX curves), y-polarized fields in both arms (red YY curves), and x- and y-polarized fields in different arms (black XY curve). Curves in (c) and (d) were measured by selecting right-hand circular polarizations in both arms (blue RR curves), left-hand circular polarizations in both arms (red LL curves), and right-hand and left-hand circular polarizations in different arms (black XY curves). In (e) and (f), the selected components are linearly polarized at an angle of +45° in both arms (blue +45, +45 curves), –45° in both arms (red –45, –45 curves), and +45° in one arm and –45° in the other arm, respectively (black +45, –45 curves).

The intensity correlation functions obtained by filtering out the high-frequency oscillations of the curves and applying Eq. (A2) are shown in Figs. 5(b), 5(d), and 5(f). Inserting these functions into Eqs. (7–10) then yields the autocorrelation functions of the four Stokes parameters illustrated in Fig. 6(a). It can be seen that the black curve describing $\langle S_0(t)S_0(t+\tau)\rangle$ is not perfectly flat, and the red curve, representing $\langle S_1(t)S_1(t+\tau)\rangle$, does not oscillate exactly about 0. The measurement imperfections like these, however, are not important as long as the experiments are focused on obtaining the polarization time instead of some particular minor details of polarization fluctuations. Substituting the autocorrelation functions of Fig. 6(a) in Eq. (6) yields the function $\gamma_P(\tau)$, illustrated in Fig. 6(b). The obtained polarization correlation function oscillates periodically about its mean value of 0 with a beating period of 90 fs. At $\tau = 0$ it has a maximum of about 0.9, which is reasonably close to the theoretically predicted value of 1. The function decreases by a factor of 2 from its maximum value when τ increases to 15 fs. Therefore, the polarization time for the considered dual-laser light is $\tau_p = 15$ fs. Within this time, the field stays essentially polarized no matter what polarization state it attains. The corresponding polarization length of the field is $l_p = 4.5$ μm. Similar polarization-beating dynamics that we found here for a dual-laser beam would also be obtained for light with two orthogonally polarized narrow-band components selected from a stationary broadband light.

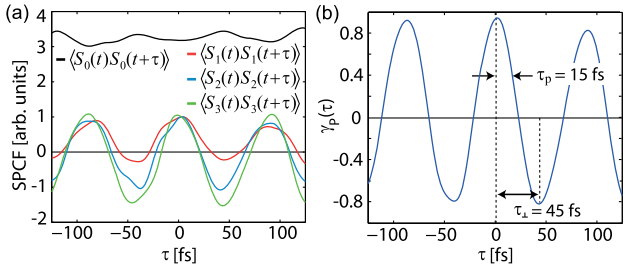

Fig. 6. Polarization dynamics of a two-laser beam. (a) Autocorrelation functions of the Stokes parameters (SPCFs) and (b) the polarization correlation function $\gamma_P(\tau)$. The polarization time τ_p is determined from $\gamma_P(\tau_p) = \gamma_P(0)/2$. The time $\tau_\perp$ is equal to the time interval within which any original polarization state of the field will be transformed into the orthogonal polarization state.

Another interesting characteristic time associated with the two-laser light is the time $\tau_\perp$, shown in Fig. 6(b). It is equal to 45 fs, which is half of the beating period. Within this time interval, any original instantaneous polarization state of the field will be transformed into the orthogonal polarization state. Indeed, this must be the case for any field composed of two monochromatic or quasi-monochromatic orthogonally polarized fields having equal amplitudes but different frequencies.

5. CONCLUSION

We have introduced a general experimental technique to characterize the polarization-state dynamics in partially polarized or unpolarized random light with femtosecond time resolution. We have verified the existence and presented the first measurements of the novel concept of polarization time that describes the rate of polarization fluctuations and gives a time interval over which a partially polarized or unpolarized light beam can be considered highly polarized. We used two-photon absorption detection combined with a polarization-selective Michelson interferometer, an approach valid for electromagnetic light, to find the polarization times of two unpolarized sources. For an ASE source and a dual-laser source, the ultrashort polarization times of 115 fs and 15 fs, respectively, were obtained. Such short polarization times are impossible to observe with traditional single-photon detection methods. The polarization time can be seen as a new concept providing additional information on random sources and propagation media, for instance, the temperature of thermal-like emitters. The polarization-state fluctuations and our technique to measure them may find a variety of applications in optics and photonics, including characterization of materials and micro- and nanostructures, research on anisotropic scattering and absorption phenomena, assessment of intra-pulse and pulse-to-pulse polarization variations, investigations of optical transitions in atoms and molecules, and nonlinear light–matter interactions, as well as quantum- and atom-optical effects concerning partially polarized waves.

APPENDIX A: TWO-PHOTON ABSORPTION SIGNAL

The two-photon absorption signal $S(\tau)$ measured in our experiment is proportional to the average of the squared intensity of the light incident on the detector. Using the complex envelope representation for the fields from the two arms of the interferometer, we find that [26]

$$\begin{aligned} S(\tau) \propto \langle I^2(t)\rangle &= \langle I_1^2(t)\rangle + \langle I_2^2(t)\rangle + 2\langle I_1(t) I_2(t+\tau)\rangle \\ &\quad + 2\langle |\mathbf{A}_1^{\mathrm{T}}(t)\mathbf{A}_2^{*}(t+\tau)|^2\rangle + \mathrm{Re}[F^{(1)}(\tau)e^{-\mathrm{i}\omega_0\tau}] \\ &\quad + \mathrm{Re}[F^{(2)}(\tau)e^{-2\mathrm{i}\omega_0\tau}], \end{aligned} \tag{A1}$$

where the vectors $\mathbf{A}_1(t)$ and $\mathbf{A}_2(t)$ are the slowly varying amplitudes of the light from arms 1 and 2, respectively, and $I_1(t)$ and $I_2(t)$ are the related instantaneous intensities. In addition, ω_0 is a frequency within the spectrum, $F^{(1)}(\tau)$ and $F^{(2)}(\tau)$ are slowly varying functions of τ, whose explicit expressions, however, are not important here, and Re denotes the real part. We seek the intensity correlation function $\langle I_1(t) I_2(t+\tau)\rangle$ included in the two-photon absorption signal. This is obtained by filtering the high-frequency components around ω_0 and $2\omega_0$, assuming that the fields in the arms have the desired polarization states specified by the wave plates and polarizers, and by developing the term with $\mathbf{A}_1(t)$ and $\mathbf{A}_2(t)$ in Eq. (A1). This procedure yields the intensity correlation functions of the various polarization states in the form

$$\langle I_{1i}(t) I_{2j}(t+\tau)\rangle = C[S_{ij}(\tau) - S_{1i} - S_{2j}]/\eta_{ij}, \tag{A2}$$

where $I_{mi}(t)$ is the instantaneous intensity of $i \in (x, y, +45, -45, \mathrm{RCP}, \mathrm{LCP})$ polarized component in arm $m \in (1, 2)$ and $S_{mi} = \langle I_{mi}^2(t)\rangle$ is the related two-photon absorption signal. Further, C is a coefficient independent of the polarization state, while $\eta_{ij} = 4$ for $i = j$ and $\eta_{ij} = 2$ if $i \neq j$. Thus, for any electromagnetic beam entering the interferometer, the intensity correlation functions of Eqs. (7–10) are obtained as $C_{i,j}(\tau) = D\langle I_{1i}(t) I_{2j}(t+\tau)\rangle$, where D is a polarization-independent constant. The coefficients C and D are finally removed, since the polarization correlation function $\gamma_{\mathrm{P}}(\tau)$ eventually evaluated from Eq. (5) is a normalized quantity.

Funding. Suomen Akatemia (268705); Itä-Suomen Yliopisto (UEF) (930350).

Acknowledgment. The authors thank Timo Vahimaa and Pertti Pääkkönen for their help in constructing the interferometer.

REFERENCES

1. P. Réfrégier, T. Setälä, and A. T. Friberg, "Maximal polarization order of random optical beams: reversible and irreversible polarization variations," Opt. Lett. **37**, 3750–3752 (2012).
2. K. Lindfors, A. Priimagi, T. Setälä, A. Shevchenko, A. T. Friberg, and M. Kaivola, "Local polarization of tightly focused unpolarized light," Nat. Photonics **1**, 228–231 (2007).
3. T. Setälä, A. Shevchenko, M. Kaivola, and A. T. Friberg, "Polarization time and length for random optical beams," Phys. Rev. A **78**, 033817 (2008).
4. A. Shevchenko, T. Setälä, M. Kaivola, and A. T. Friberg, "Characterization of polarization fluctuations in random electromagnetic beams," New J. Phys. **11**, 073004 (2009).
5. T. Voipio, T. Setälä, A. Shevchenko, and A. T. Friberg, "Polarization dynamics and polarization time of random three-dimensional electromagnetic fields," Phys. Rev. A **82**, 063807 (2010).
6. J. P. Gordon and H. Kogelnik, "PMD fundamentals: polarization mode dispersion in optical fibers," Proc. Natl. Acad. Sci. USA **97**, 4541–4550 (2000).
7. A. P. Bates, K. I. Hopcraft, and E. Jakeman, "Particle shape determination from polarization fluctuations of scattered radiation," J. Opt. Soc. Am. A **14**, 3372–3378 (1997).
8. I. Hajnsek, E. Pottier, and S. R. Cloude, "Inversion of surface parameters from polarimetric SAR," IEEE Trans. Geosci. Remote Sens. **41**, 727–744 (2003).
9. Z. Zhu and T. G. Brown, "Experimental studies of polarization properties of supercontinua generated in a birefringent photonics crystal fiber," Opt. Express **12**, 791–796 (2004).
10. L. Z. Liu, K. O'Keeffe, and S. M. Hooker, "Quasi-phase-matching of high-order-harmonic generation using polarization beating in optical waveguides," Phys. Rev. A **85**, 053823 (2012).
11. H. F. Hofmann and O. Hess, "Polarization fluctuations in vertical-cavity surface-emitting lasers: a key to the mechanism behind polarization stability," Quantum Semiclass. Opt. **10**, 87–96 (1998).
12. M. Virte, K. Panajotov, H. Thienpoint, and M. Sciamanna, "Deterministic polarization chaos from a laser diode," Nat. Photonics **7**, 60–65 (2013).
13. G. D. VanWiggeren and R. Roy, "Communication with dynamically fluctuating states of light polarization," Phys. Rev. Lett. **88**, 097903 (2002).
14. M. Coles, "The state of the universe," Nature **433**, 248–256 (2005).
15. J. M. Kovac, E. M. Leitch, C. Pryke, J. E. Carlstrom, N. W. Halverson, and W. L. Holzapfel, "Detection of polarization in the cosmic microwave background using DASI," Nature **420**, 772–787 (2002).
16. D. Mesa, C. Baccigalupi, G. De Zotti, L. Gregorini, K.-H. Mack, M. Vigotti, and U. Klein, "Polarization properties of extragalactic radio sources and

their contribution to microwave polarization fluctuations," Astron. Astrophys. **396**, 463–471 (2002).
17. B. W. Shore, *The Theory of Coherent Atomic Excitation* (Wiley, 1990).
18. A. Shevchenko, M. Kaivola, and J. Javanainen, "Spin-degenerate two-level atoms in on-resonance partially polarized light," Phys. Rev. A **73**, 035801 (2006).
19. L. S. Froufe-Pérez and R. Carminati, "Lifetime fluctuations of a single emitter in a disordered nanoscopic system: the influence of the transition dipole orientation," Phys. Stat. Sol. **205**, 1258–1265 (2008).
20. D. Colas, L. Dominici, S. Donati, A. A. Pervishko, T. C. H. Liew, I. A. Shelykh, D. Ballarini, M. de Giorgi, A. Bramati, G. Gigli, E. del Valle, F. P. Laussy, A. V. Kavokin, and D. Sanvitto, "Polarization shaping of Poincaré beams by polariton oscillations," Light: Sci. Appl. **4**, e350 (2015).
21. A. Mohan, M. Felici, P. Gallo, B. Dwir, A. Rudra, J. Faist, and E. Kapon, "Polarization-entangled photons produced with high-symmetry site-controlled quantum dots," Nat. Photonics **4**, 302–306 (2010).
22. B. R. Mollow, "Two-photon absorption and field correlation functions," Phys. Rev. **175**, 1555–1563 (1968).
23. R. Loudon, *The Quantum Theory of Light*, 3rd ed. (Oxford University, 2000).
24. J. M. Roth, T. E. Murphy, and C. Xu, "Ultrasensitive and high-dynamic-range two-photon absorption in a GaAs photomultiplier tube," Opt. Lett. **27**, 2076–2078 (2002).
25. A. Hayat, A. Nevet, P. Ginzburg, and M. Orenstein, "Applications of two-photon processes in semiconductor photonic devices: invited review," Semicond. Sci. Technol. **26**, 083001 (2011).
26. A. Shevchenko, M. Roussey, A. T. Friberg, and T. Setälä, "Ultrashort coherence times in partially polarized stationary optical beams measured by two-photon absorption," Opt. Express **23**, 31274–31285 (2015).
27. F. Boitier, A. Godard, E. Rosencher, and C. Fabre, "Measuring photon bunching at ultrashort timescale by two-photon absorption in semiconductors," Nat. Phys. **5**, 267–270 (2009).
28. F. Boitier, A. Godard, N. Dubreuil, P. Delaye, C. Fabre, and E. Rosencher, "Photon extrabunching in ultrabright twin beams measured by two-photon counting in a semiconductor," Nat. Commun. **2**, 425–426 (2011).
29. A. Nevet, A. Hayat, and M. Orenstein, "Ultrafast pulse compression by semiconductor two-photon gain," Opt. Lett. **35**, 3877–3879 (2010).
30. A. M. Weiner, *Ultrafast Optics* (Wiley, 2009).
31. S. Hooker and C. Webb, *Laser Physics* (Oxford University, 2010).
32. C. Brosseau, *Fundamentals of Polarized Light: A Statistical Optics Approach* (Wiley, 1998).
33. M. D. Dvorak, W. A. Schroeder, D. R. Andersen, A. L. Smirl, and B. S. Wherrett, "Measurement of the anisotropy of two-photon absorption coefficients in zincblende semiconductors," IEEE J. Quantum Electron. **30**, 256–268 (1994).